ACS BIO & MED CHEM Au
AN OPEN ACCESS JOURNAL OF THE AMERICAN CHEMICAL SOCIETY

pubs.acs.org/biomedchemau
Article

Intrinsically Disordered Ku Protein-Derived Cell-Penetrating Peptides

Biswanath Maity, Hariharan Moorthy, and Thimmaiah Govindaraju*

Cite This: ACS Bio Med Chem Au 2023, 3, 471−479
Read Online

ACCESS | Metrics & More | Article Recommendations | Supporting Information

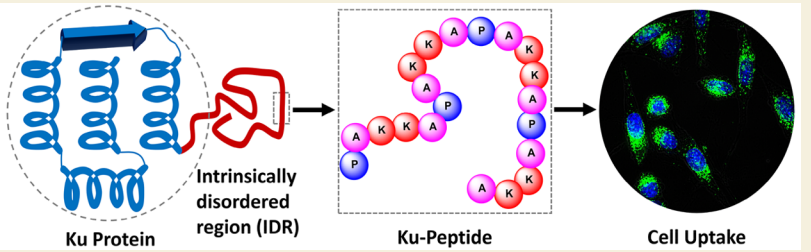

ABSTRACT: Efficient delivery of bioactive ingredients into cells is a major challenge. Cell-penetrating peptides (CPPs) have emerged as promising vehicles for this purpose. We have developed novel CPPs derived from the flexible and disordered tail extensions of DNA-binding Ku proteins. Ku-P4, the lead CPP identified in this study, is biocompatible and displays high internalization efficacy. Biophysical studies show that the proline residue is crucial for preserving the intrinsically disordered state and biocompatibility. DNA binding studies showed effective DNA condensation to form a positively charged polyplex. The polyplex exhibited effective penetration through the cell membrane and delivered the plasmid DNA inside the cell. These novel CPPs have the potential to enhance the cellular uptake and therapeutic efficacy of peptide-drug or gene conjugates.

KEYWORDS: *Cell penetrating peptide, intrinsically disordered protein, biocompatibility, DNA binding, gene delivery*

1. INTRODUCTION

Delivering active ingredients into cells effectively remains a significant challenge in realizing their biological activity. The lipid bilayer of the cell membrane acts as a semipermeable filter that permits the passage of hydrophobic hormones, water, and small uncharged molecules.[1] Transporters present in the membrane facilitate the transport of glucose, ions, and other hydrophilic nutrients.[2] However, delivering hydrophilic molecules, proteins, DNA, and other large molecules effectively is a challenging task.[3] The negative charge of DNA and its low enzymatic stability are major concerns for gene therapy in the treatment of inherited disorders, viral infections, and cancer.[4,5] Many delivery vectors such as polymers, liposomes, dendrimers, exosomes, and cell-penetrating peptides (CPPs) have been developed for efficient DNA delivery.[6−13] These vectors are designed to interact with DNA, shield its negative charges, protect it from enzymatic degradation, and facilitate its safe delivery into cells. While viral vectors are efficient in delivering DNA, they can cause immunotoxicity and genotoxicity. Similarly, nonviral vectors such as cationic polymers and liposomes can induce toxicity in cells.[14] In this context, CPPs have emerged as effective tools for delivering active ingredients through biological membranes.[15,16]

Since the discovery of the protein transduction domain in the transactivator of transcription protein in 1988, numerous natural and synthetic peptides have evolved as CPPs.[17,18] These CPPs are diverse polycationic peptides or protein domains with amino acid sequences ranging from 5 to 40.[19] The well-established chemical synthesis and easy structural modulation of CPPs provide significant advantages over other delivery vehicles. The natural occurrence of amino acids ensures the biocompatibility of CPPs, making them superior delivery agents.[20] The intracellular delivery of various therapeutic cargoes by CPPs has been extensively studied in the biomedical field.[21−25] Most CPPs contain positively charged arginine and lysine residues that interact with negatively charged lipids or carbohydrates present in the cell membrane through electrostatic interactions, facilitating their cellular entry. Peptide−membrane interactions increase the local concentration in the vicinity and enhance uptake. Many cationic CPPs are typically present in disordered coil conformations in their native state but undergo transformation into ordered secondary conformations upon interaction with the cell membrane.[26] This structural transformation upon interaction with the membrane aids in facilitating cellular

Received: May 23, 2023
Revised: October 8, 2023
Accepted: October 9, 2023
Published: October 31, 2023

translocation of certain CPPs. However, peptide folding associated with enhanced self-association on the membrane layer can induce potent membrane lytic behavior, limiting its applicability as a delivery vehicles.

We have selected intrinsically disordered proteins (IDPs) as a source to identify a new class of potent CPPs.[27,28] IDPs are proteins that lack well-defined three-dimensional conformations and play crucial roles in macromolecular recognition, signaling, and compartmentalization through their interactions with other proteins and nucleic acids.[29,30] These proteins exhibit unique properties such as low sequence complexity, poor hydrophobicity, high net charges, and repeated amino acid sequences.[31−34] Studies have shown that proteins such as nucleoid-associated protein (Hu protein) and nonhomologous DNA end-joining Ku protein contain IDP sequences at the C-terminal regulate DNA binding affinity.[35−37] Additionally, the IDP sequences in heparin-binding extracellular protein hemagglutinin aid in mycobacterium pathogenesis through interaction with host epithelial cells containing negatively charged heparan sulfate proteoglycans.[38] Inspired by the functional activities of these IDPs, we designed and synthesized a set of intrinsically disordered peptides containing AAKKA and PAKKA repeat sequences for evaluation as potential CPPs (Figure 1). One of these peptides, Ku-P4, has demonstrated good cell membrane penetration and cytocompatibility. Further studies have shown that Ku-P4 forms cationic DNA polyplexes that exhibit effective cell penetration and transfection efficiency.

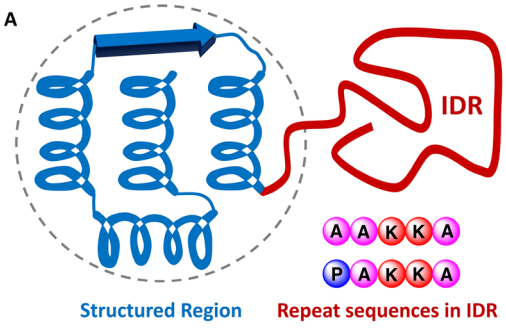

B

Ku-peptides	Peptide Sequence	Positive charges
Ku-A1	AAKKA	3
Ku-A2	AAKKAAAKKA	5
Ku-A3	AAKKAAAKKAAAKKA	7
Ku-A4	AAKKAAAKKAAAKKAAAKKA	9
Ku-P1	PAKKA	3
Ku-P2	PAKKAPAKKA	5
Ku-P3	PAKKAPAKKAPAKKA	7
Ku-P4	PAKKAPAKKAPAKKAPAKKA	9

Figure 1. (A) Schematic representation of the Ku protein with the structural conformation. The N-terminal folded region and C-terminal intrinsically disordered region (IDR). The IDR structure consists of AAKKA and PAKKA repeat sequences. (B) Peptides with variable repeats of AAKKA and PAKKA derived from the C-terminal disordered tail region of Ku protein that are selected for study as potential CPPs.

2. RESULT AND DISCUSSION

2.1. Design and Synthesis of Peptides Derived from Ku Protein

The disordered regions of intrinsically disordered proteins (IDPs) play a vital role in interactions between proteins and nucleic acids. These regions, which make up 70% of the tail domains of IDPs, are essential for regulatory functions through protein−DNA interactions. The lysine-rich cationic C-terminal of the Ku protein has a significant regulatory role in DNA compaction and chromatin organization.[27,28] It acts as an affinity tuner and facilitates sequence-specific interactions with DNA. Molecular recognition by IDPs involves conformational selection, flexibility modulation, competitive binding, and tethering. The flexible disordered region consisting of proline (P), alanine (A), and lysine (K) is known as the PAK-tail of DNA binding proteins (Figure 1A). It is commonly observed among three evolutionary IDP types: constrained disorder, nonconserved disorder, and intrinsically disorder. The conserved disordered region with a repeat of a few amino acids results from the rapid evolution in these sequences. PAK tails are widespread in bacterial proteomes but not common in human proteomes, except for histone proteins.

In eukaryotic proteomes, PAK tails are found in histone proteins and possess functional similarity with bacterial histone-like proteins and nucleoid-associated proteins.[26] The electrostatic interaction between negatively charged phospholipids and lysine residues of the PAK-tail affect membrane rearrangements to allow its delivery into the cell. The distinctive characteristics of PAK tails have prompted us to evaluate their ability to penetrate membranes, bind to DNA, and facilitate the delivery of cargo within cells. The size and charge density of peptides are critical factors in DNA delivery and transfection efficacy. In this study, we selected two series of peptides from the C-terminus of the Ku protein with PAKKA and AAKKA repeats to identify a potential CPP candidate with superior membrane penetration ability, plasmid DNA compaction, and delivery (Figure 1B). The peptides were synthesized using standard Fmoc solid-phase peptide synthesis (SPPS) protocols and labeled with 5,6-carboxyfluorescein (CF) at the N-terminal to evaluate their proficiency in penetrating cell membranes. Peptide purification was performed using reverse phase high performance liquid chromatography (RP-HPLC), and their integrity was confirmed by high-resolution mass spectroscopy (HRMS) or matrix-assisted laser desorption ionization (MALDI) mass analysis.

2.2. Secondary Structure Analysis

The secondary structure of the peptides was evaluated using circular dichroism (CD) spectroscopy in phosphate buffered saline (PBS, 10 mM, pH 7.4). Ku-A4 and Ku-P4 in PBS exhibited broad negative Cotton effects from 216 to 190 nm and a positive Cotton effect between 230 and 216 nm, indicating a random coil conformation in PBS (Figure 2A, B).[39,40] CD spectroscopy of peptides was also performed in zwitterionic and anionic model lipid membranes in PBS. The Ku-P4 peptide displayed no characteristic change in the CD signal in either zwitterionic 1,2-dipalmitoyl-*sn*-glycero-3-phosphocholine (DPPC) or anionic 1,2-dipalmitoyl-*sn*-glycero-3-phospho-*rac*-1-glycerol (DPPG) + DPPC lipid membranes and remained mostly in a disordered random coil conformation (Figure 2A). The bulky and hydrophobic proline residue increases the hydration of its own and adjacent amino

https://doi.org/10.1021/acsbiomedchemau.3c00032
ACS Bio Med Chem Au 2023, 3, 471−479

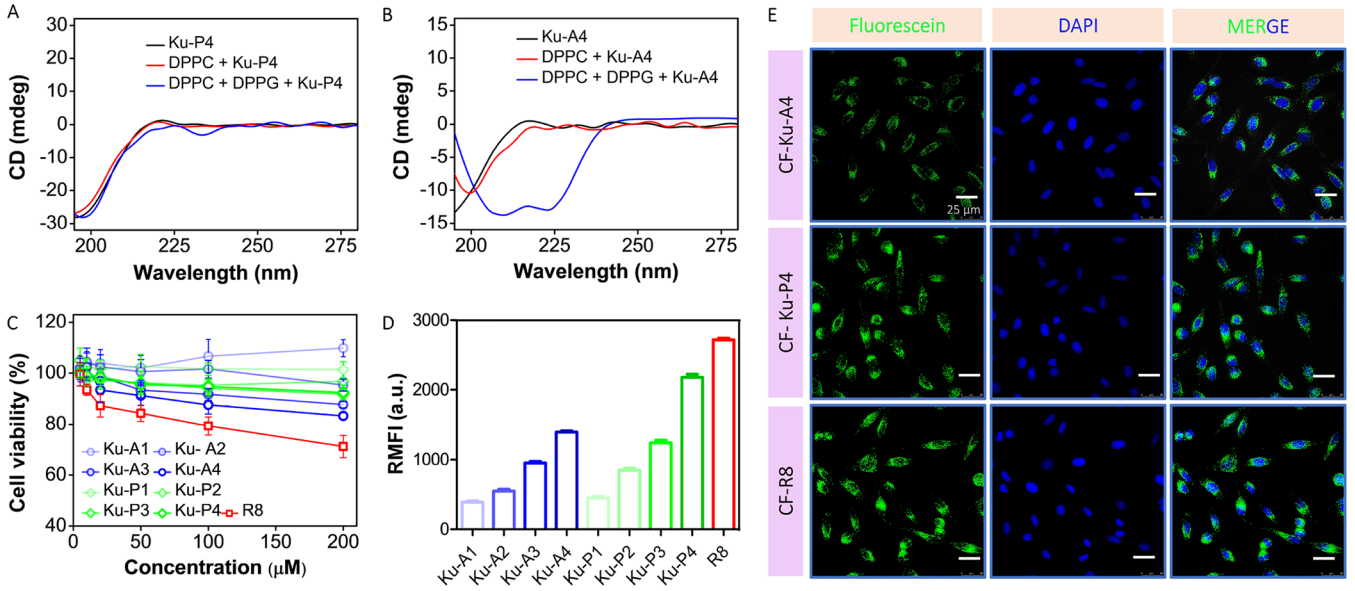

Figure 2. (A) CD spectra of Ku-P4 in PBS (10 mM, pH 7.4) containing zwitterionic (DPPC) and anionic (DPPC+DPPG) model lipid membrane. The Ku-P4 retains its native conformation in both model lipid membranes. (B) CD spectra of Ku-A4, demonstrating Ku-A4 adopts a helical conformation in the presence of DPPC+DPPG lipid membrane. (C) Viability of L929 cells in the presence of 1−200 μM of Ku-peptides at 24 h incubation. The cell viability remains more than 90% even at 200 μM concentration of all PAKKA series peptides. Relatively the cell viability declined in Ku-A3 and Ku-A4 peptides. While stearyl-R8 showed a gradual decrease in cell viability with increasing concentrations. (D) FACS analysis of peptide uptake (10 μM) in L929 cells after 6 h incubation. Peptides Ku-A4 and Ku-P4 showed comparable cell membrane penetration to the R8 peptide. (E) Fluorescence microscope images of cellular distribution by Ku-A4, Ku-P4, and CF-R8 in L929 cells (10 μM). Ku-A4 and Ku-P4 effectively penetrated the cell membrane and distributed into the cytoplasm (scale bar: 25 μm).

acids in the backbone, which impedes the hydration of the peptide side chain and restricts conformational transition.[32] In contrast, a significant conformational transition of the Ku-A4 peptide was observed with an anionic lipid membrane (Figure 2B). The characteristic Cotton effect of random coil conformations diminished, and a dominant negative Cotton effect at 222 and 210 nm was observed, which infers transformation of Ku-A4 peptide into an ordered helical conformation. The alanine residue does not play a significant role in preserving intrinsically disordered conformations,[41] whereas the proline inhibits peptide folding in membrane proximity.

2.3. Cytocompatibility Assessment

The biocompatibility of Ku-peptides was assessed to determine their suitability for use in cells. All Ku-peptides exhibited excellent biocompatibility in the L929 cell line with cell viability remaining above 90% at concentrations ranging from 10 to 200 μM which indicates their relatively nontoxic nature. However, longer sequences of AAKKA peptides Ku-A3 and Ku-A4 showed slight toxicity at higher concentrations, with cell viability declining to 87% and 80%, respectively, at a concentration of 200 μM. This decrease in cell viability is consistent with the structural transformation of these peptides from random coil to helical conformation in negatively charged lipid membranes, as observed in CD analysis. The commercially available arginine (R)-rich stearyl-R_8 peptide exhibited considerable toxicity, with cell viability reduced to 70% at a concentration of 200 μM (Figure 2C).[42] The cell viability study confirmed the excellent cytocompatibility of Ku-P4 and its potential utility in cellular experiments.

2.4. Cellular Uptake

The cell penetration efficacy of Ku-peptides in L929 cells was evaluated by using FACS analysis. A nontoxic concentration of 10 μM was selected for the cellular uptake studies of all Ku-peptides. The uptake profile showed that Ku-A4 and Ku-P4 had superior cell penetration ability compared to those of other Ku-peptides in the series. The uptake of Ku-P4 was greater than that of Ku-A4 and comparable to the control peptide R8, which is rich in arginine (Figure 2D). The higher cell membrane permeability of Ku-P4 and Ku-A4 is due to the presence of more lysine residues in the peptide backbone and peptide length. The superior membrane permeation efficacy of cytocompatible Ku-P4 is attributed to its hydrophobic proline residues, rigidity, and conformational stabilization.[39]

Fluorescence microscopy was used to visualize the internalization pattern of peptides. Ku-A4 and Ku-P4 efficiently entered into the cells compared to other peptides in the series and were distributed throughout the cytosol and nucleus while imaged after fixing the L929 cells (Figure 2E). Whereas peptides are mostly distributed in the cytoplasm of the live L929 cell (Figure S1). In contrast, other Ku-peptides did not effectively penetrate the cell membrane (Figure S2). The presence of more lysine residues in the peptide backbone of Ku-P4 and Ku-A4 played a significant role in their uptake.

To understand the cellular uptake mechanism, cellular uptake has been studied under two different treatment conditions (temperature dependent and energy depletion). The cellular uptake drastically reduced to 18% and 11% at 4 °C in Ku-A4 and Ku-P4 peptides (Figure S3A). The decline of the cellular uptake at low temperatures is attributed to the reduced membrane dynamics due to the lower environmental kinetic energy. The energy depletion by NaN_3 reduced the peptide uptake by 38% and 35% for Ku-A4 and Ku-P4 peptides (Figure S3B), indicating the uptake can be affected in energy depletion conditions. In addition, the involvement of specific endocytosis pathways has been scrutinized through the application of various endocytosis inhibitors. The macropinocytosis inhibitor

https://doi.org/10.1021/acsbiomedchemau.3c00032
ACS Bio Med Chem Au 2023, 3, 471−479

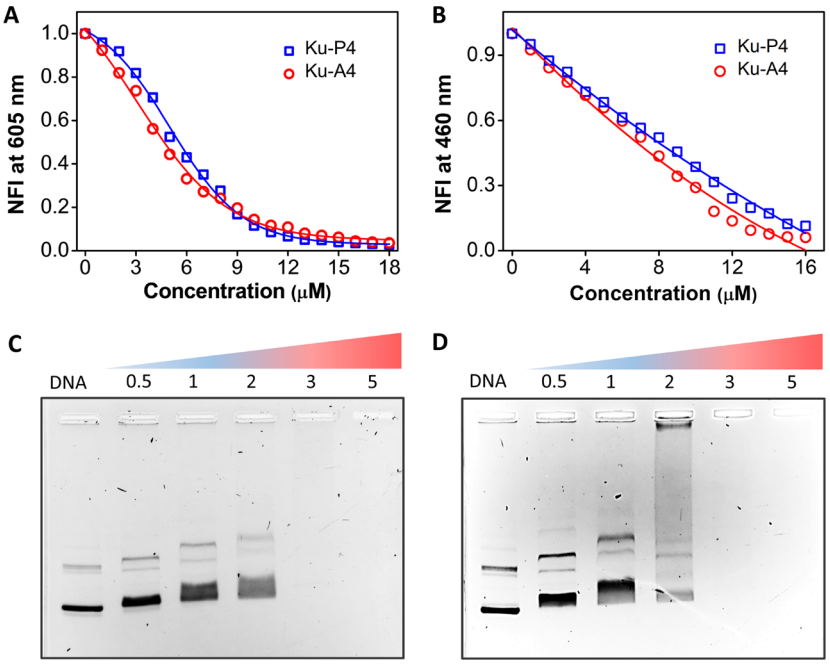

Figure 3. (A) Fluorescence quenching of intercalator dye EtBr and ctDNA complex upon titration with successive additions of Ku-A4 and Ku-P4 ligand. (B) Changes in fluorescence intensity of the minor groove binder Hoechst and ctDNA complex by Ku-A4 and Ku-P4. The fluorescence quenching study suggests effective DNA binding by peptide and displacement of the fluorescence dye. Agarose gel electrophoretic analysis for polyplex formation of Ku-A4 (C) and Ku-P4 (D) with plasmid DNA.

amiloride inhibited the cellular uptake of Ku-A4 and Ku-P4 by 48% and 39%, respectively (Figure S3C). Similarly, the clathrin-mediated endocytosis inhibitor hypertonic sucrose inhibited the cellular uptake by 49% and 35%, respectively (Figure S3D). These findings suggest that peptide uptake is contingent upon both membrane translocation and energy-dependent endocytosis.

2.5. DNA Binding Studies

The promising cellular uptake of Ku-P4 and Ku-A4 led us to investigate their ability to deliver plasmid DNA into cells. The DNA binding efficacy of Ku-peptides was evaluated using a DNA-bound dye displacement assay (Figure S4A).[43,44] Ku-peptides have positively charged lysine residues in their sequence that can interact with the negatively charged phosphate backbone of DNA through electrostatic and hydrogen bonding interactions. Ethidium bromide (EtBr), a DNA intercalating dye, exhibits significantly higher fluorescence when bound to DNA than in its free state due to stable intercalation between hydrophobic DNA base pairs, which restricts it to a planar conformation. In DNA-bound state, EtBr has a strong emission at 607 nm, which was titrated by the sequential addition of Ku-peptides. Upon stepwise addition of 1 μM Ku-peptides, EtBr fluorescence declined due to its displacement from DNA. Significant quenching of EtBr fluorescence was observed with minimal concentration variations for Ku-A4 and Ku-P4 (Figure S4B, C). Complete EtBr displacement was observed at 15 μM Ku-A4 and Ku-P4 peptide (Figure 3A). However, complete fluorescence quenching of EtBr for Ku-A3 and Ku-P3 was observed at 150 and 200 μM, respectively (Figure S5). Peptides Ku-A1, Ku-A2, Ku-P1, and Ku-P2 did not show significant DNA binding ability (Figure S6). The EtBr displacement was attributed to the strong interaction between the peptide and the DNA phosphate backbone.

Peptide binding transforms DNA conformations into a compact structure and reduces the distance between the base pairs. As a result, the intercalator dye EtBr is unable to fit between the base pairs and is displaced from DNA. The apparent binding constant (Table S1) suggests that peptides Ku-A4 and Ku-P4 have excellent DNA binding propensity. DNA binding ligands can interact with DNA in its minor and major grooves. While proteins are known to bind to the major grooves of DNA, peptides prefer the minor groove as an ideal binding site. We studied the groove binding ability using the Hoechst dye displacement assay (Figure S7A).[27] Hoechst, a bisbenzimide dye, is known to interact with the minor grooves of DNA and exhibits enhanced fluorescence at 460 nm upon binding. Hoechst-bound ctDNA was titrated with sequential additions of peptides, and the fluorescence at 460 nm was monitored. Peptide binding interferes with Hoechst binding at DNA minor groove sites, resulting in a reduction of fluorescence at 460 nm (Figure S7B, C). Peptides Ku-A4 and Ku-P4 completely displaced Hoechst at concentrations of 10 and 12 μM, respectively, due to their interaction with DNA through lysine units (Figure 3B). The apparent binding constant (Table S2) indicates that both peptides Ku-A4 and Ku-P4 possess excellent DNA minor groove binding affinity. Hoechst displacement from DNA grooves confirmed peptide binding in the minor groove and the transformation of DNA into a compact structure. Thus, dye displacement studies imply strong binding affinity of peptides Ku-A4 and Ku-P4 for DNA and condensation into compact structures.

Peptide-DNA complexation was visualized using an agarose gel electrophoresis mobility shift assay. Circular plasmid DNA (pDNA, 4.7 kb, 200 ng) was treated with varying concentrations of peptides and incubated at 4 °C for 3 h. These samples were loaded onto a 1% agarose gel in 10 mM TBE buffer, and electrophoresis was performed at 140 V for 1 h. The DNA band was visualized by staining with EtBr.

https://doi.org/10.1021/acsbiomedchemau.3c00032
ACS Bio Med Chem Au 2023, 3, 471−479

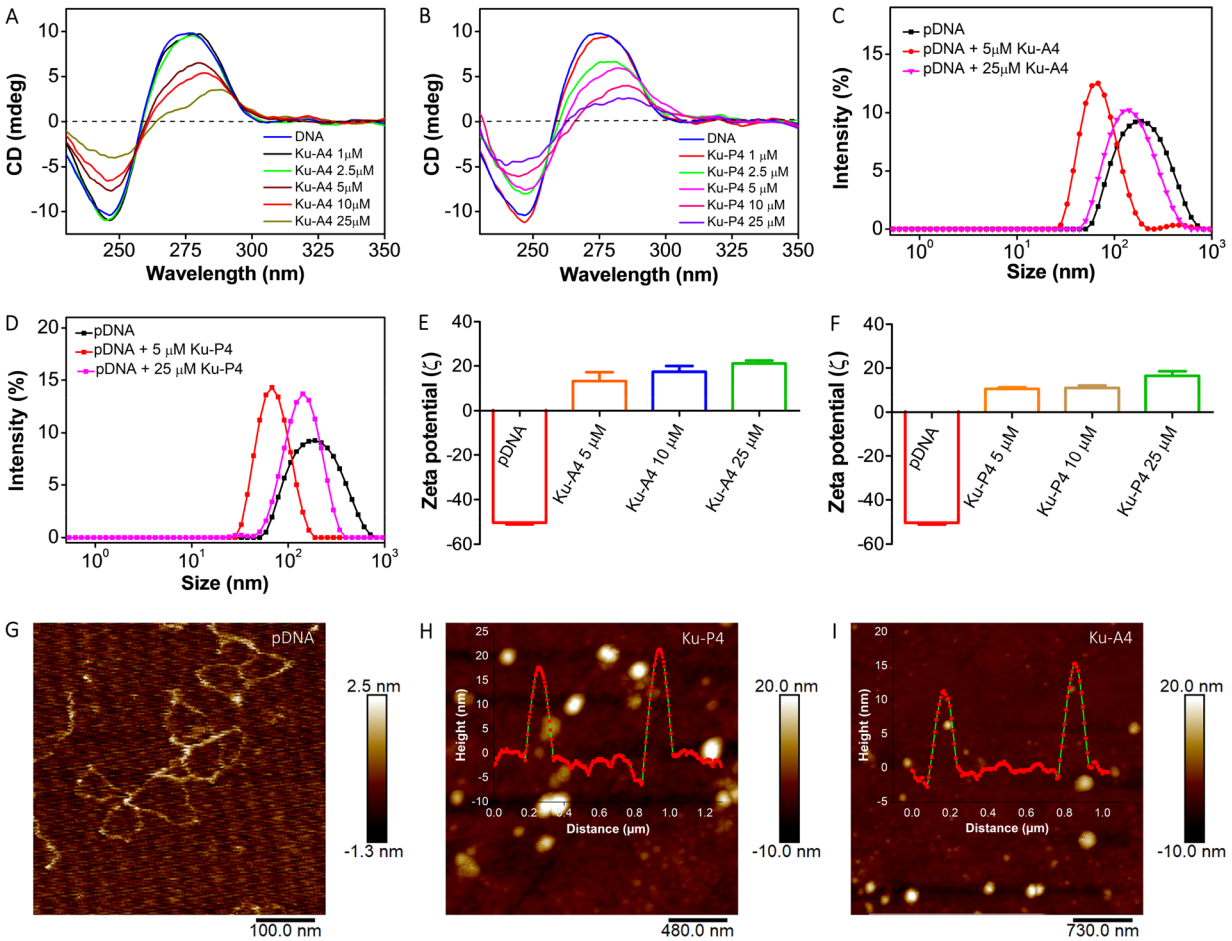

Figure 4. (A, B) CD spectra of the ctDNA with increasing Ku-A4 and Ku-P4 concentrations. The positive Cotton band intensity of double helical ctDNA at 270 nm gradually declined with increased peptide concentration due to DNA compaction. (C, D) The hydrodynamic size of the free plasmid DNA was calculated at different concentrations of Ku-A4 and Ku-P4. Interactions between peptides and DNA compact the DNA. (E, F) ζ-potential of the DNA and polyplex formed after condensation of the DNA by peptides. Peptide binding transformed the negatively charged DNA to a positively charged polyplex. AFM images of the pDNA (G) and polyplexes with 25 μM Ku-P4 (H) and Ku-A4 (I). The AFM images illustrate the nanoparticle nature of polyplexes.

Plasmid DNA typically shows three bands in agarose gel electrophoresis, corresponding to its supercoiled, open circular, and linear forms. Upon binding with the peptide, the movement of DNA toward the positively charged electrode was retarded (Figure 3C, D). With increasing peptide concentrations, the intensity of the DNA band decreased and completely disappeared due to DNA condensation. Peptides Ku-A4 and Ku-P4 showed complete condensation of DNA at a concentration of 3 μM (Figure S8). The dragging of DNA bands after the addition of peptide indicates electrostatic interactions between the peptide (lysine units) and the DNA phosphate backbone.[45] Thus, the peptides Ku-A4 and Ku-P4 have strong binding interactions with DNA and are promising DNA condensing agents.

The conformational transition of DNA upon peptide binding was determined by using CD spectroscopy. Double-stranded ctDNA exhibits a negative Cotton effect at 245 nm corresponding to backbone helicity and a positive Cotton effect at 275 nm arising from nucleobase $\pi-\pi$ stacking in B-conformation. As the peptide concentration increased, the ellipticity at 275 nm gradually decreased along with a concomitant redshift of the signal due to the interaction of peptides with ctDNA (Figure 4A, B).[46,47] The negative Cotton effect at 245 nm also moderately decreased with an increasing peptide concentration, indicating helicity distortion upon peptide binding. These results correlated with displacement assay data obtained by using the minor groove binding Hoechst dye. The ctDNA CD Cotton effect pattern indicates that the B-conformation was preserved in a compact form after the peptide interaction. Although agarose gel retardation studies showed DNA condensation at a concentration of 3 μM Ku-peptides, complete compaction of DNA required 25 μM of peptides. This suggests that complete condensation of ctDNA at a concentration of 25 μM peptide transforms it into condensates.

The size and charge of the polyplex formed by Ku-peptides were characterized using a combination of dynamic light scattering (DLS) and ζ-potential measurements. pDNA (50 ng/mL) in Tris-HCl buffer (10 mM, pH 7.4) was treated with different concentrations of Ku-A4 and Ku-P4 and incubated at 4 °C for 3 h. pDNA alone exhibited a hydrodynamic size of 180 nm due to its unorganized random structure (Figure 4C). At a concentration of 5 μM peptide, DNA conformation becomes organized into condensed polyplex architectures, and the hydrodynamic radius reduces to 70 nm (Figure 4C, D). The size of the polyplex further increased to 140 nm at higher peptide concentrations, possibly due to further deposition of peptides in the condensate. The size distribution of the

https://doi.org/10.1021/acsbiomedchemau.3c00032
ACS Bio Med Chem Au 2023, 3, 471−479

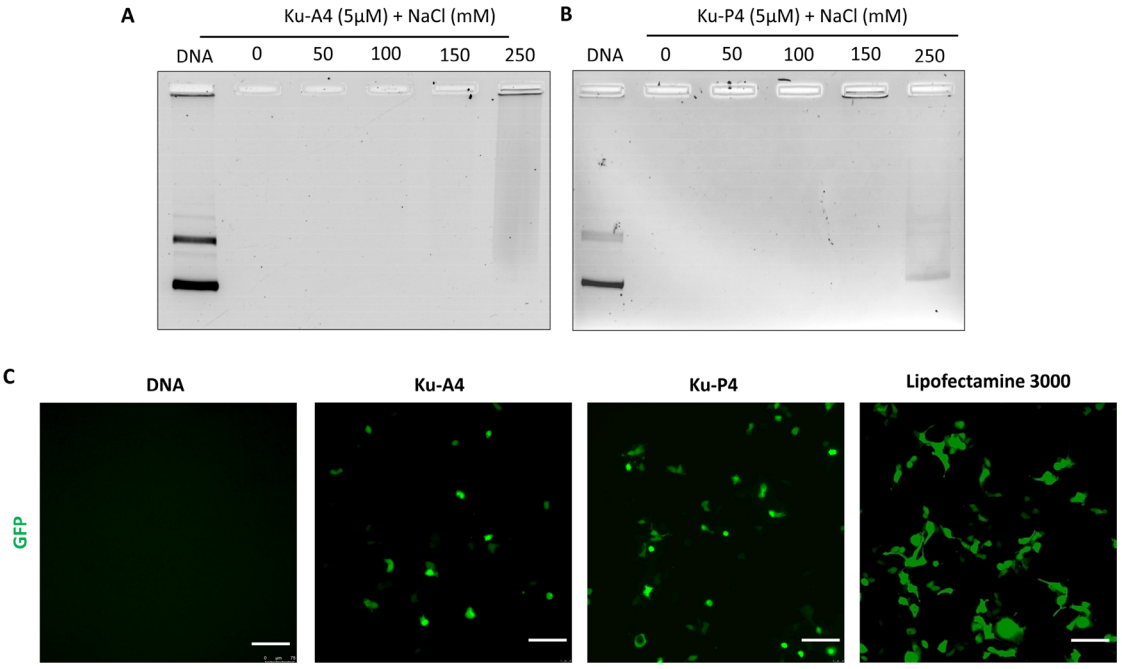

Figure 5. DNA polyplex stability of Ku-A4 (A) and Ku-P4 (B) at varying NaCl concentration. Polyplexes are stable at biological salt concentration, while it starts disassembling at 250 mM of NaCl. (C) Fluorescence microscopy images of pEGFP-C2 plasmid DNA transfected HEK-293T cell using the peptides Ku-A4, Ku-P4 and Lipofectamine-3000. The GFP fluorescence in cells discloses effective delivery of plasmid DNA inside the cell by using Ku-peptides and further expression of GFP protein inside the cell. (Scale bar: 100 μM.)

polyplex was similar for both Ku-A4 and Ku-P4. The ζ-potential measurements showed charge reversal of negatively charged DNA upon binding with positively charged peptide. DNA (200 ng/mL) exhibited a potential of −50.33 mV, which increased to +10.56 mV at a concentration of 5 μM Ku-A4 and further increased to +16.4 at 25 μM (Figure 4E). Peptide Ku-A4 also showed a ζ-potential of +13.20 at a concentration of 5 μM, which further increased to +21.1 at 25 μM (Figure 4F). DLS studies indicate that Ku-peptides transformed unorganized random DNA structures into compact condensed particles. The observed positive ζ potential of the polyplex will enhance cellular uptake through the negatively charged cell membrane.

The nature of DNA condensates was further investigated by using atomic force microscopy (AFM). Free plasmid DNA displayed a thread-like morphology due to its unstructured fiber-like structure (Figure 4G). Interestingly, peptides condensed DNA into nanoarchitectures with diameters ranging from 110 to 160 nm (Figure 4H, I). This result confirmed the structural transformation of DNA upon binding with Ku-peptides. No free DNA structure was observed in the presence of the Ku-A4 and Ku-P4. All biophysical studies correlated to the DNA compaction ability of Ku-A4 and Ku-P4. The nanoarchitectured polyplex with high surface positive charges is anticipated to enable efficient cellular uptake and successful DNA delivery.

The stability of polyplexes in biological media is crucial for their DNA transfection efficiency. Interactions with proteins and ions in the media can destabilize the polyplexes, leading to DNA degradation by nuclease enzymes. To assess polyplex stability, an agarose gel retardation assay was performed using different concentrations of a sodium chloride (NaCl) solution. Polyplexes were formed by condensing pDNA (150 ng) with Ku peptides (25 μM) and treated with NaCl solution. The sample was incubated further for 6 h and loaded in agarose gel well, and gel electrophoresis was performed at 140 V for 1 h (Figure 5A, B). The results showed that the polyplexes were stable up to 150 mM NaCl, indicating strong DNA binding with peptides and the minimization of premature DNA release. However, at 250 mM NaCl, the polyplexes became unstable and began to release DNA. This reversible binding is essential for condensation followed by decondensation of DNA after delivery inside the cell. The time dependent average particle size distribution through DLS studies indicates the particles are stable over time (Figure S9). Thus, a highly water-soluble peptide with dynamic DNA binding stabilizes the particle sizes and prevents the higher order aggregate formation. The Z-average value and polydispersity index (PDI) of the polyplex does not change significantly in the presence of serum (Figure S10), indicating the stable polyplex formation. Furthermore, the stability of the polyplex with the DNase was evaluated by an agarose gel retardation assay. The free DNA completely degraded in the presence of DNase after 2 h of incubation (Figure S11). In contrast, the polyplex was stable, as observed in the agarose gel retardation assay, suggesting the stability of the polyplex (Figure S11). Further DNase was heat inactivated at 80 °C for 10 min followed by the addition of heparin to induce decondensation. In the presence of heparin, decondensed DNA was observed similar to the native form indicating the ability of the peptide polyplex to protect DNA from enzymatic degradation. Importantly, we have also shown that the polyplex is highly stable even at higher temperatures. Therefore, the polyplex is stable enough to achieve the successful entry of the DNA into the cell.

2.6. Plasmid DNA Transfection

The formation of stable DNA polyplexes with positive ζ-potential encouraged us to evaluate Ku-A4 and Ku-P4 peptides as DNA transfection agents. Before DNA transfection the cytocompatibility of the polyplex was evaluated in HEK 293T

https://doi.org/10.1021/acsbiomedchemau.3c00032
ACS Bio Med Chem Au 2023, 3, 471−479

cell. Cells were treated with varying concentrations of peptide polyplex, cultured for 24 h and viability was evaluated by using MTT assay. No considerable change in cell viability was observed even at 100 μM Ku-P4 peptide polyplex complex, and cell viability remains >90% (Figure S12). Thus, the polyplex of the intrinsically disordered peptide is nontoxic and can be used for the plasmid DNA transfection. The plasmid transfection study was performed in HEK 293T cells, which are commonly used for such studies. Polyplexes of plasmid DNA pEGFP-C2 with Ku-A4 and Ku-P4 peptide were prepared in optiMEM media and added to cells in low serum concentration (2% FBS). The expression of the green fluorescent protein (GFP) was visualized by green fluorescence emission. pDNA alone was unable to penetrate the cell membrane due to its negative charge, resulting in no GFP expression. However, in the presence of pDNA/Ku-P4 and pDNA/Ku-A4 polyplex, GFP expressions were observed inside the cell after 48 h of incubation (Figure 5C). The Ku-P4 peptide demonstrated a greater efficacy than the Ku-A4 peptide, supporting its superior membrane permeability. However, the transfection efficacy observed by the Ku-peptides are lower than the commercially available lipofectamine 3000 (Figure 5C). Despite the relatively low transfection efficiency of Ku-peptides, the lower toxicity profile presents an opportunity for further development into superior transfection agents.

3. CONCLUSION

In conclusion, we have identified a novel cell-penetrating peptide derived from the IDR of the natural DNA binding Ku protein. The developed Ku-P4 peptide is cytocompatible and exhibits a good cell membrane permeability. Biophysical studies suggest that the presence of a proline residue is crucial for maintaining the intrinsic disorder state of the peptide and biocompatibility. Ku-P4 demonstrated excellent DNA binding ability and stabilization and compact DNA into nanoarchitectures. These DNA-peptide polyplexes (nanoarchitectures) with a positive ζ-potential effectively delivered plasmid DNA through the negatively charged cell membrane, which resulted in good transfection efficiency. Thus, Ku-peptides could be further developed as delivery vehicles for nucleic acids and cell-impermeable drugs.

4. MATERIALS AND METHODS

4.1. Peptide Synthesis

Ku-peptides were synthesized using the standard 9-fluorenylmethyloxycarbonyl (Fmoc) solid phase peptide synthesis (SSPS) protocol on rink amide resin. The efficacy of amino acid coupling and Fmoc deprotection was monitored using the Kaiser test. After peptide sequences were completed, the peptide and amino acid side chains were cleaved using a cocktail solution containing trifluoroacetic acid (TFA):triisopropyl silane (TIPS):DCM (95:2.5:2.5) for 3 h at room temperature. The resulting solution was collected and treated with cold ether to obtain a white precipitate. The peptides were purified using RP-HPLC on a C18 column with an acetonitrile/water mobile phase and characterized by MALDI-TOF and HRMS (Q-TOF). Peptide purity was analyzed using an HPLC chromatogram and peptide purity >95% was used for experiments.

4.2. CD Spectroscopy Studies

The CD spectra of Ku-peptides were obtained using a Jasco J-810 spectropolarimeter in 10 mM PBS (pH 7.4). Peptide samples were incubated for 24 h prior to scanning, and spectra were recorded from 350 to 190 nm in a 1 mm quartz cuvette with a bandwidth of 1 nm. Spectra were collected three times, and blank spectra were subtracted. Artificial lipid membranes were prepared using dipalmitoylphosphatidylcholine (DPPC), dipalmitoylphosphoglycerol (DPPG), and cholesterol. Zwitterionic membranes were prepared using a DPPC:Cholesterol ratio of 70:30, while negatively charged lipid membranes were prepared using a DPPC:DPPG:Cholesterol ratio of 70:20:10. Lipids were solubilized in a chloroform:methanol mixture to make a 2 mM stock solution, and solvents were evaporated using nitrogen gas and vacuum to form lipid films. The films were hydrated in PBS buffer and vortexed for 30 min to create a lipid emulsion. The emulsion was subjected to freeze−thaw cycles and stored at 4 °C for further use. Peptides were mixed with lipids in a 1:50 ratio and incubated at 37 °C for 6 h before CD experiments were performed.

4.3. Cytotoxicity Studies

The cytotoxic effect of Ku-peptides on L929 cells was assessed using a colorimetric MTT assay. L929 cells were cultured in Dulbecco's modified Eagle's medium (DMEM) supplemented with 10% fetal bovine serum (FBS), and 1% penicillin-streptomycin (PS). Cells were seeded at a density of 1×10^4 cells/well in a 96-well plate and cultured for 24 h. Cells were then treated with peptide solutions at concentrations ranging from 20 to 200 μM and incubated for an additional 24 h. MTT solution (10 μL of 0.5%) was added and further incubated for 4 h before the supernatant was carefully removed without disturbing the formazan crystals. The crystals were dissolved in 100 μL of dimethyl sulfoxide: methanol (1:1) mixture, and the absorbance of the formazan dye was measured at a wavelength of 570 nm using a SpectroMax i3x microplate reader, with background correction at 690 nm.

4.4. Cellular Uptake Studies

The intracellular localization of Ku-peptides in L929 cells was quantified by using fluorescence-activated cell sorting (FACS) analysis. L929 cells were seeded at a density of 50×10^4 cells/well in a 12-well plate, cultured for 24 h, and treated with 10 μM of CF-labeled peptides for 6 h. Cell wells are washed with PBS (10 mM, pH = 7.4) and detached from wells using 0.25% trypsin. The cell pellet was washed with PBS three times, and the cellular uptake was analyzed. For fluorescence analysis by microscopy, L929 cells were plated in confocal disk at density of 2×10^4 and cultured for 24 h. Fluorophore labeled peptide solution (10 μM) was treated and incubated for 6 h. Unbound peptides were removed by washing with 10 mM PBS solution and fixed with 4% paraformaldehyde, and the cell nucleus was stained with DAPI. Images were captured using a Leica DMi8 fluorescence microscope.

4.5. DNA Binding Studies

Fluorescence spectral measurements were conducted using an Agilent Cary Eclipse fluorescence spectrophotometer. Briefly, 4 μM intercalator dye ethidium bromide (EtBr) was incubated with 100 μM ctDNA for 6 h and titrated with increased peptide concentration. The EtBr fluorescence was recorded on excitation at 526 nm and emission from 555 to 700 nm. The fluorescence measurement was continued until the EtBr fluorescence is saturated.

4.6. Agarose Gel Electrophoresis Mobility Shift Assay

Green fluorescence protein plasmid DNA (200 ng) was incubated at room temperature with different concentrations of peptides for 45 min in Tris.HCl buffer (10 mM, pH = 7.4) to form the condensates. The solutions were mixed with 2 μL of loading dye (20% glycerol, 25 mM EDTA, and 0.05% bromophenol blue and xylene cyanol) and transferred into wells. Electrophoresis was performed in TBE buffer at 140 V for 1 h. For polyplex stability studies, 2 μL of various NaCl concentrations was mixed with the polyplex solutions, incubated at 37 °C for 3 h, and loaded into the gel well.

4.7. DNA Conformational Analysis

The CD spectra of ct-DNA in the presence of the peptides were performed for the conformation changes during the condensation. To ct-DNA (100 μM) in Tris buffer, peptide solution (0−50 μM) was added and incubated for 45 min at room temperature. The spectrum

https://doi.org/10.1021/acsbiomedchemau.3c00032
ACS Bio Med Chem Au 2023, 3, 471−479

was collected from 350 to 200 nm in a 1 cm quartz cuvette using a Jasco-810 spectropolarimeter.

4.8. DLS Studies

eGFP plasmid DNA (200 ng) was mixed with peptide solution (0−25 μM) and incubated at room temperature for 45 min. The sample was transferred into the fluorescence quartz cuvette of path length 1 cm, and measurement was performed in Malvern Zetasizer nano-ZS.

4.9. AFM Analysis

The nature of the polyplex condensates formed by Ku-peptide-DNA complexation was further characterized by AFM analysis. Briefly, 10 mM $NiCl_2$ was drop cast on a freshly cleaved mica sheet, kept for 10 min and wiped out with filter paper. 40 μL of eGFP plasmid DNA (1 ng/μL in Tris.HCl buffer) was transferred into the activated mica sheet and further incubated for 20 min. The aliquot was removed with filter paper, washed three times with 100 μL of filtered Milli Q water, and kept at 37 °C for drying. The polyplex samples were drop casted without activation of the mica surface. Imaging was performed with a Bruker Bioscope Resolve microscope at a scanning rate of 1 Hz using a 3 nm probe. Images were further processed with the NanoScope analysis software.

4.10. eGFP Plasmid DNA Isolation and Purification

Enhanced plasmid DNA pEGFP-C2 (4.7 kb) was isolated from *E. coli* DH5α and purified using a Qiagen miniprep plasmid isolation kit. The concentration of pEGFP was determined using nanoDrop in a SpectraMax i3x microplate reader. The purity was checked from the absorbance ratio at 260 and 280 nm.

4.11. eGFP Plasmid DNA Transfection

The eGFP plasmid DNA transfection experiment was performed to check the DNA delivery efficacy of Ku-peptides in HEK 293T cells. In a solution of eGFP plasmid (200 ng) in optiMEM, a Ku-peptide (50 μM) solution was added dropwise and mixed properly through gentle vertexing. The mixture was kept at room temperature for 45 min to form the condensed polyplex structure. The polyplex sample was transferred to 70% confluent 48-cell wells containing 2% FBS without antibiotics. After 12 h of incubation, the cultured medium was replaced with fresh medium and further cultured for 72 h, and green fluorescence protein (GFP) expression was imaged under a Leica Dim8 fluorescence microscope.

■ ASSOCIATED CONTENT

Supporting Information

The Supporting Information is available free of charge at https://pubs.acs.org/doi/10.1021/acsbiomedchemau.3c00032.

Materials, cellular uptake mechanism, polyplex stability, cytotoxicity, cellular uptake study, mechanism of cellular uptake, emission profile for EtBr and hoechst dye displacement, binding constant table, quantification of agarose gel retardation, polyplex stability, serum stability, DNase stability, polyplex cytotoxicity, eGFP transfection, and characterization data of peptides (PDF)

■ AUTHOR INFORMATION

Corresponding Author

Thimmaiah Govindaraju − *Bioorganic Chemistry Laboratory, New Chemistry Unit, and School of Advanced Materials (SAMat), Jawaharlal Nehru Centre for Advanced Scientific Research (JNCASR), Bengaluru 560064 Karnataka, India;* orcid.org/0000-0002-9423-4275; Email: tgraju@jncasr.ac.in

Authors

Biswanath Maity − *Bioorganic Chemistry Laboratory, New Chemistry Unit, and School of Advanced Materials (SAMat), Jawaharlal Nehru Centre for Advanced Scientific Research (JNCASR), Bengaluru 560064 Karnataka, India*

Hariharan Moorthy − *Bioorganic Chemistry Laboratory, New Chemistry Unit, and School of Advanced Materials (SAMat), Jawaharlal Nehru Centre for Advanced Scientific Research (JNCASR), Bengaluru 560064 Karnataka, India*

Complete contact information is available at: https://pubs.acs.org/10.1021/acsbiomedchemau.3c00032

Author Contributions

T.G. conceived, designed, and supervised the project. B.M. performed experiments. T.G. and B.M. analyzed the data. B.M. and T.G. wrote and revised the manuscript. H.M. contributed to revision of the manuscript.

Notes

The authors declare no competing financial interest.

■ ACKNOWLEDGMENTS

The authors thank JNCASR, Science and Engineering Research Board (core grant: CRG/2020/004594), New Delhi, India, and Sheikh Saqr Laboratory (SSL), ICMS-JNCASR for financial support, B.M. and H.M. acknowledge CSIR for fellowship, Dr. Rajasekhar for guidance in peptide synthesis.

■ REFERENCES

(1) Oren, I.; Fleishman, S. J.; Kessel, A.; Ben-Tal, N. Free diffusion of steroid hormones across biomembranes: A simplex search with implicit solvent model calculations. *Biophys. J.* **2004**, *87*, 768−779.

(2) Cooper, G. M. *The cell: A molecular approach*, 2nd ed.; Sinauer Associates: Sunderland, MA, 2000.

(3) Mitragotri, S.; Burke, P. A.; Langer, R. Overcoming the challenges in administering biopharmaceuticals: Formulation and delivery strategies. *Nat. Rev. Drug Discovery* **2014**, *13*, 655−672.

(4) Biffi, A.; Montini, E.; Lorioli, L.; Cesani, M.; Fumagalli, F.; Plati, T.; Baldoli, C.; Martino, S.; Calabria, A.; Canale, S.; et al. Lentiviral hematopoietic stem cell gene therapy benefits metachromatic leukodystrophy. *Science* **2013**, *341*, 1233158.

(5) Yang, J.; Hendricks, W.; Liu, G.; McCaffery, J. M.; Kinzler, K. W.; Huso, D. L.; Vogelstein, B.; Zhou, S. A nanoparticle formulation that selectively transfects metastatic tumors in mice. *Proc. Natl. Acad. Sci. U. S. A.* **2013**, *110*, 14717−14722.

(6) Kirtane, A. R.; Panyam, J. Polymer nanoparticles: Weighing up gene delivery. *Nat. Nanotechnol.* **2013**, *8*, 805−806.

(7) Pack, D. W.; Hoffman, A. S.; Pun, S.; Stayton, P. S. Design and development of polymers for gene delivery. *Nat. Rev. Drug. Discovery* **2005**, *4*, 581−593.

(8) Pattni, B. S.; Chupin, V. V.; Torchilin, V. P. New developments in liposomal drug delivery. *Chem. rev.* **2015**, *115*, 10938−10966.

(9) Yang, J.; Zhang, Q.; Chang, H.; Cheng, Y. Surface engineered dendrimers in gene delivery. *Chem. Rev.* **2015**, *115*, 5274−5300.

(10) Alvarez-Erviti, L.; Seow, Y.; Yin, H.; Betts, C.; Lakhal, S.; Wood, M. J. A. Delivery of siRNA to the mouse brain by systemic injection of targeted exosomes. *Nat. Biotechnol.* **2011**, *29*, 341−345.

(11) Gopal, V. Bioinspired peptides as versatile nucleic acid delivery platforms. *J. Controlled Release* **2013**, *167*, 323−332.

(12) Suh, J. S.; Lee, J. Y.; Choi, Y. S.; Chong, P. C.; Park, Y. J. Peptide-mediated intracellular delivery of miRNA-29b for osteogenic stem cell differentiation. *Biomaterials* **2013**, *34*, 4347−4359.

(13) Kichler, A.; Leborgne, C.; Danos, O.; Bechinger, B. Characterization of the gene transfer process mediated by histidine-rich peptides. *J. Mol. Med.* **2007**, *85*, 191−201.

(14) Juliano, R. L.; Ming, X.; Nakagawa, O. Cellular uptake and intracellular trafficking of antisense and siRNA oligonucleotides. *Bioconjugate Chem.* **2012**, *23*, 147−157.
(15) Torchilin, V. P. Cell penetrating peptide-modified pharmaceutical nanocarriers for intracellular drug and gene delivery. *Biopolymers* **2008**, *90*, 604−610.
(16) Plank, C.; Tang, M. X.; Wolfe, A. R.; Szoka, F. C. Branched cationic peptides for gene delivery: role of type and number of cationic residues in formation and in vitro activity of DNA polyplexes. *Hum. Gene Ther.* **1999**, *10*, 319−332.
(17) Frankel, A. D.; Pabo, C. O. Cellular uptake of the tat protein from human immunodeficiency virus. *Cell* **1988**, *55*, 1189−1193.
(18) Vives, E.; Brodin, P.; Lebleu, B. A truncated HIV-1 Tat protein basic domain rapidly translocates through the plasma membrane and accumulates in the cell nucleus. *J. Biol. Chem.* **1997**, *272*, 16010−16017.
(19) Heitz, F.; Morris, M. C.; Divita, G. Twenty years of cell-penetrating peptides: From molecular mechanisms to therapeutics. *Br. J. Pharmacol.* **2009**, *157*, 195−206.
(20) Habault, J.; Poyet, J. L. Recent advances in cell penetrating peptide-based anticancer therapies. *Molecules* **2019**, *24*, 927.
(21) Wadia, J. S.; Stan, R. V.; Dowdy, S. F. Transducible TAT-HA fusogenic peptide enhances escape of TAT-fusion proteins after lipid raft macropinocytosis. *Nat. Med.* **2004**, *10*, 310−315.
(22) Madhu, C.; Voshavar, C.; Rajasekhar, K.; Govindaraju, T. Cyclic dipeptide based cell-penetrating peptidomimetics for effective DNA delivery. *Org. Biomol. Chem.* **2017**, *15*, 3170−3174.
(23) Okuda, A.; Tahara, S.; Hirose, H.; Takeuchi, T.; Nakase, I.; Ono, A.; Takehashi, M.; Tanaka, S.; Futaki, S. Oligoarginine-bearing tandem repeat penetration-accelerating sequence delivers protein to cytosol via caveolae-mediated endocytosis. *Biomacromolecules* **2019**, *20*, 1849−1859.
(24) Akishiba, M.; Takeuchi, T.; Kawaguchi, Y.; Sakamoto, K.; Yu, H.-H.; Nakase, I.; Takatani-Nakase, T.; Madani, F.; Graslund, A.; Futaki, S. Cytosolic antibody delivery by lipid-sensitive endosomolytic peptide. *Nat. Chem.* **2017**, *9*, 751−761.
(25) Takayama, K.; Hirose, H.; Tanaka, G.; Pujals, S.; Katayama, S.; Nakase, I.; Futaki, S. Effect of the attachment of a penetration accelerating sequence and the influence of hydrophobicity on octaarginine-mediated intracellular delivery. *Mol. Pharmaceutics* **2012**, *9*, 1222−1230.
(26) Eiriksdottir, E.; Konate, K.; Langel, U.; Divita, G.; Deshayes, S. Secondary structure of cell-penetrating peptides controls membrane interaction and insertion. *Biochim. Biophys. Acta Biomembr.* **2010**, *1798*, 1119−1128.
(27) Walker, J. R.; Corpina, R. A.; Goldberg, J. Structure of the Ku heterodimer bound to DNA and its implications for double-strand break repair. *Nature* **2001**, *412*, 607−614.
(28) Boehr, D. D.; Nussinov, R.; Wright, P. E. The role of dynamic conformational ensembles in biomolecular recognition. *Nat. Chem. Biol.* **2009**, *5*, 789−796.
(29) Salerno, P.; Larsson, J.; Bucca, G.; Laing, E.; Smith, C. P.; Flardh, K. One of the two genes encoding nucleoid-associated HU proteins in streptomyces coelicolor is developmentally regulated and specifically involved in spore maturation. *J. Bacteriol.* **2009**, *191*, 6489−6500.
(30) Vuzman, D.; Levy, Y. Intrinsically disordered regions as affinity tuners in protein-DNA interactions. *Mol. BioSyst.* **2012**, *8*, 47−57.
(31) Rado-trilla, N.; Alba, M. Dissecting the role of low-complexity regions in the evolution of vertebrate proteins. *BMC Evol. Biol.* **2012**, *12*, 155.
(32) Coletta, A.; Pinney, J. W.; Solıs, D. W. Y.; Marsh, J.; Pettifer, S. R.; Attwood, T. K. Low-complexity regions within protein sequences have position-dependent roles. *BMC Syst. Biol.* **2010**, *4*, 43.
(33) Uversky, V. N.; Gillespie, J. R.; Fink, A. L. Why are "natively unfolded" proteins unstructured under physiologic conditions? *Proteins: Struct., Funct., Genet.* **2000**, *41*, 415−427.
(34) Jorda, J.; Xue, B.; Uversky, V. N.; Kajava, A. V. Protein tandem repeats - the more perfect, the less structured. *FEBS J.* **2010**, *277*, 2673−2682.
(35) Khare, H.; Dey, D.; Madhu, C.; Senapati, D.; Raghothama, S.; Govindaraju, T.; Ramakumar, S. Conformational heterogeneity in tails of DNA-binding proteins is augmented by proline containing repeats. *Mol. BioSyst.* **2017**, *13*, 2531−2544.
(36) Mukherjee, A.; Bhattacharyya, G.; Grove, A. The C-terminal domain of HU-related histone-like protein Hlp from mycobacterium smegmatis mediates DNA end-joining. *Biochemistry* **2008**, *47*, 8744−8753.
(37) Bhowmick, T.; Ghosh, S.; Dixit, K.; Ganesan, V.; Ramagopal, U. A.; Dey, D.; Sarma, S. P.; Ramakumar, S.; Nagaraja, V. Targeting Mycobacterium tuberculosis nucleoid-associated protein HU with structure-based inhibitors. *Nat. Commun.* **2014**, *5*, 4124.
(38) de Lima, C. S.; Marques, M. A. M.; Debrie, A. S.; Almeida, E. C. C.; Silva, C. M. A.; Brennan, P. J.; Sarno, E. N.; Menozzi, F. D.; Pessolani, M. C. V. Heparin-binding hemagglutinin (HBHA) of Mycobacterium leprae is expressed during infection and enhances bacterial adherence to epithelial cells. *FEMS Microbiol. Lett.* **2009**, *292*, 162−169.
(39) Sadler, K.; Eom, K. D.; Yang, J. L.; Dimitrova, Y.; Tam, J. P. Translocating proline-rich peptides from the antimicrobial peptide bactenecin. *Biochemistry* **2002**, *41*, 14150−14157.
(40) Lopes, J. L. S.; Miles, A. J.; Whitmore, L.; Wallace, B. A. Distinct circular dichroism spectroscopic signatures of polyproline II and unordered secondary structures: Applications in secondary structure analyses. *Protein Sci.* **2014**, *23*, 1765−1772.
(41) Macarthur, M. W.; Thornton, J. M. Influences of proline residues on protein conformation. *J. Mol. Biol.* **1991**, *218*, 397−412.
(42) Futaki, S.; Ohashi, W.; Suzuki, T.; Niwa, M.; Tanaka, S.; Ueda, K.; Harashima, H.; Sugiura, Y. Stearylated arginine-rich peptides: A new class of transfection systems. *Bioconjugate Chem.* **2001**, *12*, 1005−1011.
(43) Jenkins, T. C. Optical absorbance and fluorescence techniques for measuring DNA-drug interactions. In *Drug-DNA Interaction Protocols*; Fox, K. R., Ed.; Methods in Molecular Biology; Humana Press: Totowa, 1997; Vol *90*, pp 195−218.
(44) Pratihar, S.; Suseela, Y. V.; Govindaraju, T. Threading intercalator-induced nanocondensates and role of endogenous metal ions in decondensation for DNA delivery. *ACS Appl. Bio Mater.* **2020**, *3*, 6979−6991.
(45) Prevette, L. E.; Kodger, T. E.; Reineke, T. M.; Lynch, M. L. Deciphering the role of hydrogen bonding in enhancing pDNA-polycation interactions. *Langmuir* **2007**, *23*, 9773−9784.
(46) Anuradha; Alam, M. S.; Chaudhury, N. K. Osmolyte changes the binding affinity and mode of interaction of minor groove binder hoechst 33258 with calf thymus DNA. *Chem. Pharm. Bull.* **2010**, *58*, 1447−1454.
(47) Choosakoonkriang, S.; Lobo, B. A.; Koe, G. S.; Koe, J. G.; Middaugh, C. R. Biophysical characterization of PEI/DNA complexes. *J. Pharm. Sci.* **2003**, *92*, 1710−1722.

https://doi.org/10.1021/acsbiomedchemau.3c00032
ACS Bio Med Chem Au 2023, 3, 471−479